

# **EXHIBIT A52**



# Towards a quantitative model to predict the toxicity/pathogenicity potential of mineral fibers

Alessandro F. Gualtieri\*

Chemical and Earth Sciences Department, The University of Modena and Reggio Emilia, Modena, Italy

## ARTICLE INFO

### Keywords:

Mineral fibers  
Crystal structure  
Toxicity  
Pathogenicity  
Lung cancer  
Risk assessment

## ABSTRACT

Some mineral fibers represent a health hazard because they are classified as cancer-causing chemical/physical toxicants upon (chronic) dust inhalation. Although in the last decades they have been the subject of intensive multidisciplinary investigations, the mechanisms by which mineral fibers induce toxic and pathogenic adverse effects on human health and environment are not yet fully understood. The major intricacy of the biological approach that prevents the design of a conclusive shared model of behavior of mineral fibers in a biological system stems from their very nature with intrinsic variability in chemical, molecular, structural and morphometric parameters, biodurability and surface reactivity.

This paper presents the first attempt to devise a quantitative predictive model of toxicity/pathogenicity of mineral fibers based on their physical/chemical and morphological parameters. Although the author is aware that all parameters should be measured in comparable *in vivo* systems that accurately simulate the lung and or pleural environment, this preliminary model was conceived to deliver a fiber potential toxicity/pathogenicity index (FPTI) to be integrated with the biological approach so to create a quantitative predictive model of behavior of mineral fibers in a biological system. The FPTI model is thought to be a predictive tool aimed at ranking the toxicity and pathogenicity potential of fibers like asbestos or unregulated/unclassified mineral fibers. It may eventually be applied to other materials like man-made synthetic fibers and elongated mineral particles (EMP). Work is in progress to revise and validate the model in joint collaboration with international competent organizations, and to deliver a FPTI model-based user-friendly code.

## 1. Introduction

Mineral dust includes natural fibers like asbestos (chrysotile and fibrous amphiboles) and the fibrous zeolite erionite (Baumann et al., 2013). The group of amphibole asbestos consists of five species: actinolite asbestos  $\text{Ca}_2(\text{Mg,Fe})_5\text{Si}_8\text{O}_{22}(\text{OH})_2$ , tremolite asbestos  $\text{Ca}_2\text{Mg}_5\text{Si}_8\text{O}_{22}(\text{OH})_2$ , anthophyllite asbestos  $(\text{Mg,Fe}^{2+})_7\text{Si}_8\text{O}_{22}(\text{OH})_2$ , crocidolite  $\text{Na}_2(\text{Fe}^{2+},\text{Mg})_3\text{Fe}_2^{3+}\text{Si}_8\text{O}_{22}(\text{OH})_2$  and amosite  $(\text{Fe}^{2+},\text{Mg})_7\text{Si}_8\text{O}_{22}(\text{OH})_2$ . Amphiboles are double-chain silicates with a Si(Al):O ratio of 4:11. The oxygen atoms of the chains can coordinate Si (Al) and a variety of other cations: the C cations ( $\text{Mg}^{2+}$ ,  $\text{Fe}^{2+}$ ,  $\text{Mn}^{2+}$ ,  $\text{Al}^{3+}$ ,  $\text{Fe}^{3+}$ ,  $\text{Ti}^{3+}$ ,  $\text{Ti}^{4+}$ ,  $\text{Li}^+$ ,  $\text{Mn}^{3+}$ ), the B cations ( $\text{Na}^+$ ,  $\text{Li}^+$ ,  $\text{Ca}^{2+}$ ,  $\text{Mn}^{2+}$ ,  $\text{Fe}^{2+}$ ,  $\text{Mg}^{2+}$ ), and the A cations ( $\text{Na}^+$ ,  $\text{K}^+$ ,  $\text{Ca}^{2+}$ ,  $\text{Li}^+$ ) (Hawthorne et al., 2012). Chrysotile is the most common asbestos mineral. It is a trioctahedral hydrous layer silicate based on a 1:1 layer structure with a Si-centered tetrahedral sheet and a Mg-centered octahedral sheet. The ideal chemical formula is  $\text{Mg}_3(\text{OH})_4\text{Si}_2\text{O}_5$ . Erionite is a widespread zeolite whose framework is composed of columns of

cancrinite cages (Gualtieri et al., 1998) connected by a double six-membered ring of tetrahedra, forming hexagonal prisms. Its fibrous form has usually diagenetic origin and occurs in volcanic tuffs.

Both asbestos and fibrous erionite are included by the International Agency for Research on Cancer (IARC) in Group 1 as Carcinogen for humans (IARC, 2012; Sayan and Mossman, 2017). The classification is based upon epidemiological and *in vivo* carcinogenicity tests but is not supported by a quantitative model because to date the mechanisms by which these fibers induce adverse effects on human health and environment are still not fully understood. Hence, it is not surprising that contradictory quali-quantitative figures are found in the literature as attempts to rank the pathogenicity (carcinogenicity) and toxicity of mineral fibers. A few selected representative examples are: “In most studies, chrysotile was more ‘toxic’ than the amphiboles” (Bignon and Jaurand, 1983); “Amphiboles are more potent than chrysotile in the induction of fibrotic lung disease and associated lung cancers” (Berry and Newhouse, 1983); “Few would dispute that tremolite is more carcinogenic than chrysotile on a weight-for-weight basis, partly or perhaps largely

\* Corresponding author at: Chemical and Earth Sciences Department, The University of Modena and Reggio Emilia, Via G. Campi 103, I-41125 Modena, Italy.  
E-mail address: [alessandro.gualtieri@unimore.it](mailto:alessandro.gualtieri@unimore.it).

<https://doi.org/10.1016/j.taap.2018.05.012>

Received 18 December 2017; Received in revised form 7 May 2018; Accepted 11 May 2018

Available online 22 May 2018

0041-008X/ © 2018 Elsevier Inc. All rights reserved.

because of its greater durability” (Harrison et al., 1999); “*Erionite is more potent than crocidolite in causing mesothelioma*” (Dogan et al., 2006). The major intricacy of the biological approach that prevents the design of a quantitative model of behavior of mineral fibers in biological systems is their chameleonic nature. In fact, besides the complexity of the biochemical events governing the adverse outcome patterns leading to the malignancies, major difficulties arise from the great variability of the chemistry, molecular arrangement, size, biodegradability and surface reactivity of mineral fibers (Pollastri et al., 2014). Without a shared conclusive model describing the toxicity/pathogenicity of mineral fibers, the solution of the so called ‘global chrysotile issue’ (Carbone et al., 2007; Bernstein et al., 2013) is far to come yet. One of the consequences of such ‘global confusion’ is the never ending litigation upon the ranking of toxicity of chrysotile asbestos with respect to amphibole asbestos. As a matter of fact, amphibole asbestos species are banned worldwide while chrysotile is banned only in 28% of the countries in the world with its ‘safe use’ allowed in the others (72% in the world). Without a quantitative predictive model for the assessment of the pathogenicity and toxicity of mineral fibers, species of unknown carcinogenic potential possibly present in the natural environment or actually in use can be underestimated and cause exposure of the population.

In this scenario, a long-term research project started in Italy in 2010 with the goal to systematically classify mineral fibers with respect to their ability to cause damage to organisms (cyto- and genotoxicity) and promote molecular initiating events at the basis of carcinogenesis. All the properties that affect their toxicity and pathogenicity upon chronic inhalation have been identified and systematically investigated using a set of standard fibers (Pollastri et al., 2014, 2015 and Bursi Gandolfi et al., 2016). The assessment of the fiber potential toxicity/pathogenicity from the perspective of the invader (fiber cause) is complementary to that delivered by the biological approach which is solely focused on the invaded (organism effects).

The outcome of this long term project is the elaboration of a toxicity/pathogenicity quantitative predictive model that delivers a fiber potential toxicity/pathogenicity index (FPTI) to be combined with the biological approach so that a comprehensive quantitative model of behavior of mineral fibers in biological systems can be devised. The development of toxicity quantitative evaluation tools has become a need for all the scientific fields dealing with both natural and synthetic chemicals and toxicants such as toxicology, applied pharmacology, ecology, and environmental sciences. Several examples of toxicity quantitative evaluation models have recently appeared in these areas of the scientific literature. Although especially developed for acute toxicants, a few remarkable examples are the predictive model for the classification of the toxicity of ionic liquids (Roy and Das, 2013), the model of pesticide toxicity index (PTI), a screening tool to assess potential aquatic toxicity of complex pesticide mixtures (Nowell et al., 2014), and the model of toxic constituents index for the prediction of the hypertoxic phytomedicine (Zhang et al., 2016). In building the FPTI model, some basic concepts used in the Toxicity Estimation Software Tool (T.E.S.T.) for the estimation of the toxicity from molecular structure developed by the U.S. Environmental Protection Agency (EPA), 2012 were applied.

The predictive model to determine the FPTI can be used to assess *a priori* the potential activity of mineral fibers that are not classified so far and deliver proper plans of risk prevention. It may help to prevent new cases of mass exposure to natural fibers' health hazards such as those that occurred in Biancavilla (Italy) for fluoro-edenite and Cappadocia (Turkey) for erionite that led to peaks of malignant mesothelioma (MM) in the exposed population. Moreover, it is the road map for an experimental protocol to quantitatively assess the toxicity/pathogenicity potential of mineral fibers including physical-chemical, mineralogical, microstructural characterization, that can be a basis for *in vitro* acellular and cellular tests, and *in vivo* tests. The model may eventually be applied with proper adaptation to man-made mineral fibers or nanoparticles.

In this paper, the science beyond the model is explained and the results of the application of the model to selected mineral fibers of social and economic importance are presented and critically discussed.

## 2. The FPTI model

### 2.1. Introduction to the model

Most of the working models of toxicity existing in the literature evaluate the (acute) toxicity of a chemical, a chemical product or a natural/synthetic toxicant on the basis of the sum of quotients or coefficients in order to calculate a specific index. For example, in the case of the pesticide toxicity index of Munn et al. (2001) and Nowell et al. (2014), the sum of toxicity quotients for each pesticide compound (i) is measured for each taxonomic group (t):

$$PTI_t = \sum_{i=1}^n \frac{E_i}{TC_{i,t}}$$

where  $E_i$  is the concentration of pesticide i, n is the number of detected pesticides in an environmental sample, and  $TC_{i,t}$  is the toxicity concentration for the pesticide i for the taxonomic group t. Zhang et al. (2016) express their toxicity constituents index in weighed percentage from the equation:

$$TCI = 100 \cdot \sum_{i=1}^n \left( \frac{\frac{1}{MLD_i}}{\sum_{i=1}^n \frac{1}{MLD_i}} \right) \cdot X_i$$

with n = the number of toxicity constituents; MLD = minimum lethal dose of constituent i;  $X_i$  = the determined content of constituent i. Based on the Quantitative Structure Activity Relationships (QSARs), some mathematical models used to predict measures of toxicity from physical characteristics of the structure of chemicals rely upon molecular descriptors (Papa et al., 2007). Simple QSAR models calculate the toxicity T of chemicals using a simple linear function of molecular descriptors like:

$$T = ax_1 + bx_2 + c$$

where  $x_1$  and  $x_2$  are the independent molecular descriptor variables and a, b, and c are fitted parameters. In the FPTI model, the same concepts have been applied and an index was created with structural/physical/chemical descriptors instead of independent molecular descriptors. The descriptors in the model may be cross correlated so that a proper weighing scheme is necessary (see below).

### 2.2. The parameters of the model

Table 1 lists the parameters that cause major adverse effects leading to toxic and pathobiological processes responsible for adverse outcomes.

Although a complete description of the parameters of the model can be found in Gualtieri et al. (2017), each parameter will be shortly described in the following section.

#### 2.2.1. Morphometric parameters

The geometry of a fiber is defined by its length L (1,1) and diameter D (1,2). L is a key factor in toxicity, inflammation and pathogenicity of fibers (Donaldson et al., 2010). The ‘Stanton hypothesis’ (Stanton et al., 1981) is based on observations of experimental animals following injection and implantation of fibers, indicating that the optimum morphology for inducing intrapleural tumors by these routes of administration is  $D \leq 0.25 \mu\text{m}$  and  $L > 8 \mu\text{m}$ . Following that model, needle-shaped particles with  $L > 8 \mu\text{m}$  (so-called ‘Stanton fibers’) cannot be eliminated by phagocytic cells like macrophages (Churg, 1993), leading to a process known as “frustrated phagocytosis”. Concerning the curvature of the fibers (1,3), for cylindrical lattices like that possessed by

**Table 1**

Parameters considered in the FPTI model, their major adverse effects and related pathobiological processes responsible for adverse outcomes in carcinogenesis, and the experimental methods for their determination.

Parameter	Element	Major adverse effect	Major pathobiological process	Experimental technique used for its determination
Morphometric				
Length L	(1,1)	Frustrated phagocytosis	Inflammation and oxidative stress	SEM <sup>a</sup> /TEM <sup>b</sup>
Diameter D	(1,2)	Frustrated phagocytosis	Inflammation and oxidative stress	SEM/TEM
Crystal curvature	(1,3)	Reduced surface adhesion of proteins/cells	Inflammation and oxidative stress?	Diffraction, TEM
Crystal habit	(1,4)	Airways deposition depth	Inflammation and oxidative stress	SEM/TEM
Fiber density	(1,5)	Airways deposition depth	Inflammation and oxidative stress	Diffraction
Hydrophobic character of the surface	(1,6)	Interaction with biopolymers, phagocytosis	Inflammation and oxidative stress?	Electrophoretic mobility
Surface area	(1,7)	Airways deposition depth, frustrated phagocytosis	(chronic) inflammation and oxidative stress	BET <sup>c</sup>
Chemical				
Total iron content	(1,8)	Production of ROS	DNA damage and inflammation	EPMA <sup>d</sup>
Ferrous iron content	(1,9)	Production of ROS	DNA damage and inflammation	Mössbauer spectroscopy
Surface ferrous iron/iron nuclearity	(1,10)	Production of ROS	DNA damage and inflammation	XPS <sup>e</sup> , TOF-SIMS <sup>f</sup> (surface sensitive), FTIR <sup>g</sup> , UV-Vis <sup>h</sup>
Content of metals other than iron	(1,11)	Production of ROS	DNA damage and inflammation	XRF <sup>i</sup> , ICP-MS <sup>j</sup>
Biodurability related				
Dissolution rate log(R)	(1,12)	Frustrated phagocytosis	Inflammation and secondary genotoxicity	Acellular biodurability
Velocity of iron release	(1,13)	Production of ROS	Inflammation	EPMA + acellular biodurability
Velocity of silica dissolution	(1,14)	Production of ROS?	Oxidative stress and inflammation?	Acellular biodurability
Velocity of release of metals	(1,15)	ROS production	DNA damage, inflammation, primary and secondary genotoxicity	XRF, ICP-MS + acellular biodurability
Surface activity				
ξ potential	(1,16)	Production of ROS and hemolysis	Inflammation and primary cytotoxicity	Electrophoretic mobility
Fibers' aggregation	(1,17)	Frustrated phagocytosis	Inflammation	Electrophoretic mobility
Cation exchange in zeolites	(1,18)	Interference with ER cross-talk?	Apoptosis, necrosis?	CEC <sup>k</sup> , EPMA...

<sup>a</sup> SEM = Scanning electron microscopy.

<sup>b</sup> TEM = Transmission electron microscopy.

<sup>c</sup> BET = Brunauer-Elmet-Teller specific surface determination.

<sup>d</sup> EPMA = Electron probe micro-analysis.

<sup>e</sup> XPS = X-ray photoelectron microscopy.

<sup>f</sup> TOF-SIMS = time of flight secondary ion mass spectrometry.

<sup>g</sup> FTIR = Fourier transform infra-red spectroscopy.

<sup>h</sup> UV-Vis = UV-visible spectroscopy.

<sup>i</sup> XRF = X-ray fluorescence.

<sup>j</sup> ICP-MS = Inductively coupled plasma mass spectrometry.

<sup>k</sup> CEC = cation exchange capacity.

chrysotile, the radius of curvature is small whereas for the other lattices, the radius of curvature tends to infinite. For nanoparticles, small changes in diameter can affect protein binding and hence biological responses (Deng et al., 2012). It was also observed that protein adsorption on curved surfaces like that of chrysotile or very small nanoparticles (such as 7 nm diameter gold nanoparticles: Deng et al., 2012) is suppressed up to the point when it no longer occurs, offering a route to differential control of protein adsorption (Lynch and Dawson, 2008).

The crystal habit of a fiber (1,4) may influence its toxicity potential. Fibers may be curled or needle-like, leading to different depositional behaviors once inhaled. Compared to needle-like fibers, the curled fibers like those displayed by chrysotile tend to be deposited in the upper airways system (Harris and Timbrell, 1977). There, they come in contact with epithelial cells and may be taken up and translocated to the interstitium or cleared through the mucociliary elevator (Evans et al., 1973). The curled crystal habit thus appears to be a positive factor because fibers do not reach the alveolar regions. Hence, concerning this parameter, the pathogenicity of chrysotile should be lower than that of other needle-like fibers such as amphiboles reaching the deep lung and pleura.

The density (1,5) of a fiber is accounted for in the calculation of its aerodynamic diameter  $D_{ae}$  (Gualtieri et al., 2017). Hence, it influences the deposition depth of inhaled particles in the airways (Yeh et al.,

1976). It should be noted that the value of ideal density is of poor applicative significance as mass transport in suspension is dominated in most cases by agglomerates consisting of multiple primary particles as well as trapped suspension fluid and associated proteins (DeLoid et al., 2014).

Concerning the chemical character of the surface (1,6), there are two factors related to the hydrophilicity of the particle surface that may prompt adverse effects: capacity of adsorption of biopolymers and interaction with human phagocytic cells. Hydrophobic surfaces adsorb biopolymers more strongly than hydrophilic surfaces (van Oss et al., 1999). The hydrophobic surface allows interaction with hydrophobic domains and residues in the protein and the process occurs with a gain of entropy. In general, it was found that particles with stronger hydrophobic character are more prone to cell uptake.

The surface area (1,7) is usually defined as specific or reactive (Fischer et al., 2014). Specific area is the total surface area of a sample divided by its mass and is generally determined by gas adsorption and the Brunauer-Emmett-Teller (BET) equation (Brunauer et al., 1938). Reactive surface area is an elusive property and very hard to measure. It is often used to distinguish the portions of the surface that contribute dominantly to a measured reaction-related parameter (e.g. dissolution) from portions that do not (Rufe and Hochella Jr., 1999). Whatever the definition of surface area is, it is certainly one factor that affects

biodurability of a fiber. In particular, the dissolution rate is directly related to the surface area and is included as a factor in equations describing dissolution kinetics (see for example Fischer et al., 2014).

### 2.2.2. Chemical parameters

The way iron produces adverse effects is not yet fully understood. Such evaluation is complicated by the fact that most of the studies are performed *ex situ* and not in lung simulated environments. It has long been known that the iron content (1,8) and basically the  $\text{Fe}^{2+}$  (1,9) content at the surface of asbestos minerals promote the formation of hydroxyl radicals ( $\text{HO}^\cdot$ ) with cyto- and genotoxic effects. Content and speciation (oxidation state and coordination environment) of iron as well as intracellular iron mobilization and transport were shown to be important factors of amphibole asbestos-induced pathobiological activity (see for example, Hardy and Aust, 1995; Turci et al., 2011). The surface activity of iron as source of  $\text{HO}^\cdot$  relies on the Haber-Weiss cycle, the process responsible for the formation of  $\text{HO}^\cdot$ .  $\text{H}_2\text{O}_2$ , the radical species superoxide ( $\text{O}_2^{\cdot-}$ ) and free oxygen are released *in vivo* by the macrophages during the inflammatory burst which accompanies frustrated phagocytosis of long amphibole fibers and inflammasome activation (Kamp, 2009). To be active, iron sites must be situated at the fiber surface (1,10) in contact with the cell or cell medium. Creation of active surface sites is possible, for example due to dissolution phenomena *in vitro* and *in vivo*. In this case, the number of active iron sites is strictly correlated with the specific surface area (1,7) as well as with other dissolution-related parameters. The activity of iron as a catalytic site for the production of  $\text{HO}^\cdot$  is possible only when the surface of the mineral fiber is fresh. Aging, oxidation and protein coating neutralize surface activity and hence such chemical surface reaction involving single active sites *in vivo* must be carefully considered. The activity of iron sites is also related to their nuclearity (1,10), the number of iron atoms joined in a single coordination entity by bridging ligands indicated by monomeric (single iron atom, no other iron atoms in the second shell coordination), dinuclear or dimeric (a cluster of two iron atoms, connected by a bridging oxygen atom), trinuclear or trimeric (a cluster of three iron atoms, connected by bridging oxygen atoms), and so on. According to Zecchina et al. (2007), the sites that have been described for erionite are isolated  $(\text{FeO})^{2+}$  structures and are the preferred candidate active site  $[(\text{H}_2\text{O})_5\text{FeO}]^{2+}$  as they have a low iron nuclearity. Minor fractions of paired  $\text{Fe}^{2+}$ - $\text{Fe}^{2+}$  active species or  $\text{Fe}_x\text{O}_y$  clusters entrapped in the zeolite framework cavities are considered less active. Clustered iron, with high nuclearity should be much less active or indeed inactive. The limiting case is an iron oxide. As stated above, because (porous) coating of proteins both *in vitro* and *in vivo* neutralize surface activity, the activity related to the nuclearity of iron should also be considered and properly weighed in the model.

The content of trace elements (1,11) should be also evaluated as these elements are capable of inducing lung cancer (see for example Wei et al., 2014). There are both epidemiological and experimental indications that trace metals are carcinogenic (Nemery, 1990), and some researchers claimed that asbestos fibers may play a passive role in producing diseases as carriers of trace elements or hydrocarbons (Dixon et al., 1970). Since chrysotile is not persistent in the lungs, the possibility that trace metals are quickly released in the extracellular medium should be considered, and chrysotile asbestos samples rich in heavy metals should be carefully investigated (Bloise et al., 2016).

### 2.2.3. Biodurability related parameters

Biodurability (1,12) is defined as the resistance to chemical/biochemical alteration and is a significant contributor to biopersistence (Utembe et al., 2015). If a fiber dissolves or breaks down rapidly in lung fluids, it is assumed to have a low biopersistence and it is in principle less harmful than a biopersistent fiber. While a first order approximation of biodurability of a fiber can be determined with *in vitro* acellular studies, well designed *in vivo* studies are required to accurately assess biodurability. *In vitro* acellular studies generally use simulated lung

fluids (SLF) such as Gamble's solution (see for example Marques et al., 2011). A solution buffered at pH 7–7.4 is used to simulate the extracellular environment and a pH of 4–4.5 is used to simulate the intracellular environment (phagolysosome vacuoles engulfing the fiber during phagocytosis).

*In vivo* biopersistence studies greatly contributed to the understanding of the dissolution mechanisms and kinetics of mineral fibers (Bernstein and Pavlisko, 2017). For long fibers which cannot be fully phagocytosed by the macrophage, biopersistence is the determinant for potential toxicity. If the long fibers are biosoluble in the lung fluid, they can either dissolve or break apart into shorter fibers and be cleared. Long fibers which are not biosoluble will persist in the lung and initiate an inflammatory response. Those fibers which deposit in the alveoli adjacent to the visceral pleural wall will eventually penetrate through the *interstitium* and visceral pleural wall into the pleural cavity initiating a fibrotic response and sustained macrophage and neutrophil response. Pleural fluid clears from the pleural cavity through an array of stomata on the parietal pleural surface. Fibers which enter into the pleural cavity would follow the fluid flow towards these stomata. If fibers are too large to enter the stomata, then they would remain on the surface, accumulate and potentially elicit an inflammatory response. Longer fibers can also become blocked at the lymphatic valves. In these situations, if they are not biosoluble, they will likely initiate an inflammatory response. With biopersistent longer fibers, this inflammatory response can lead to the development of pleural fibrosis and over time neoplastic processes (Bernstein and Pavlisko, 2017).

Hence, the high biodurability of a mineral fiber such as crocidolite is responsible for chronic inflammation in the lungs whereas the low biodurability of a fiber such as chrysotile explains its (supposedly) decreased toxicity potential (Ilgren and Chatfield, 1998; Ilgren, 2008; Bernstein et al., 2008). Recently, Gualtieri et al. (2018) systematically measured *in vitro* acellular dissolution times of several samples of chrysotile and fibrous amphiboles and confirmed that the biodurability of chrysotile is significantly lower than that of the amphiboles.

The velocity of dissolution of iron (1,13) controls the amount of bulk iron that becomes available at the surface of the fibers. As we have seen above, the surface activity of  $\text{Fe}^{2+}$  can be a source of  $\text{HO}^\cdot$  during the so-called Haber-Weiss cycle. Ideally, fast dissolution of an iron-rich fiber may enhance the production of  $\text{HO}^\cdot$ . Despite the huge difference in iron content between iron-poor chrysotile and fibrous iron-rich amphiboles, the much faster dissolution rate of chrysotile compared to amphiboles prompts comparable rates of release of active surface iron in the same time.

The amount of silica-rich reactive relicts produced during the dissolution of mineral fibers (1,14) is a parameters of unpredicted effects that should be taken into account. The first step of chrysotile dissolution is a 'pseudomorphic' amorphization (Wypych et al., 2005) followed by dissolution *sensu stricto* (physical-chemical dissolution of the fibers). The formation of a silica-rich fiber skeleton after amorphization of chrysotile, characterized by silanol groups ( $\text{Si}-\text{OH}$ ) and ionized silanol groups ( $\text{Si}-\text{O}^-$ ), may prompt production of  $\text{HO}^\cdot$  (Pollastri et al., 2016). If this proviso is correct, when rating the toxicity/pathogenicity potential of a mineral fiber, one should consider the rate of production of such reactive metastable silica-rich relict during the dissolution process.

Concerning the rate of release of metals (1,15), this parameter must be carefully evaluated as many of these elements may display a catalytic surface activity, with production of  $\text{HO}^\cdot$  and other reactive species. For example, Mn acts as catalyst for the dismutation of superoxide to  $\text{H}_2\text{O}_2$ , but does not promote the formation of  $\text{HO}^\cdot$  in the presence of  $\text{H}_2\text{O}_2$  to any great extent (Halliwell, 1990).

### 2.2.4. Surface activity

Although, as already observed for other parameters (e.g. iron), the role of surface charge should be further investigated as most of the existing studies are performed *ex situ* and not in lung simulated environments, it was postulated that the surface charge of fibers, as

measured by the  $\xi$  potential (1,16), may correlate with a number of phenomena responsible for adverse effects (Gualtieri et al., 2017). According to Gabor and Anca (1975), the mechanism for haemolysis induced by the fibers depends upon their  $\xi$  potential. A negative  $\xi$  potential may prompt the formation of hydroxyl radicals in contact with peroxide and may favor the binding of collagen and redox-activated Ferrich proteins. It may also affect cross-talk phenomena and apoptosis (Pollastri et al., 2014). The  $\xi$  potential of mineral fibers at pH 4.5 and 7.0 displays values in the range  $-10$  to  $-26$  mV, with no remarkable difference between the various fiber species (Pollastri et al., 2014). At such low absolute values, particle agglomeration (1,17) is favored. This is a critical point as culture conditions having the most agglomeration induce highest biological responses (Roggli and Sharma, 2014). It is important to remark that the highest biological response in terms of frustrated phagocytosis regards the agglomeration of long fibers when they have already passed the upper airways and reached the lung/alveolar space. This concept should not be confused with the agglomeration of short tangled fibers as observed for nanotubes (NTs) that, by contrast, does not cause any significant inflammation (Kostarelos, 2008; Donaldson et al., 2010). Hence, fibers with low absolute values of  $\xi$  potential (i.e. agglomerated) are virtually more prone than fibers with high absolute values of  $\xi$  potential (i.e. stable) to cause adverse effects such as frustrated phagocytosis. Fibrous zeolites like erionite may release or exchange cations (1,18) in organic medium, interfering with cell cycles. Ballirano and Cametti (2015) observed that leaching erionite fibers with Gamble's solution induces a complex ionic-exchange process resulting in a temporary partial replacement of  $\text{Na}^+$  by  $\text{Ca}^{2+}$ . The possibility that zeolite cation exchange in the extracellular and intracellular environment prompts acute (primary) or chronic (secondary) adverse effects has not been evaluated yet.

Table 1 also reports the experimental methods required for measuring the fiber parameters. The determination of each parameter should be part of a standardized multidisciplinary experimental protocol. One of the drawbacks of this procedure is that the determination of some of the parameters like the dissolution rates can be very time consuming (months to years) especially for mineral fibers stable in acidic environment like amphibole asbestos.

### 2.3. The weighing scheme of the parameters and the model equation

The parameters of the model described in Section 2.2 can be correlated with each other. Prompted by the concept of the hierarchical clustering described in the T.E.S.T. program by the U.S. Environmental Protection Agency (EPA) (2012), a hierarchical scheme was developed for the model. Three steps were defined with the parameters of step 1 that have no correlations with the others, the parameters of step 2 that are derived from the parameters of step 1, and the parameters of step 3 that are derived from both the parameters of step 1 and 2. For example, the  $\xi$  potential is an uncorrelated step 1 character of a fiber that directly influences the hydrophobic character of the fiber surface (step 2 parameter) which in turn directly influences the fiber aggregation (step 3 parameter). Fig. 1 depicts the scheme of the hierarchical clustering of the FPTI model. A weighing scheme is associated with each parameter of the model according to its step or hierarchy H:  $w_1 = 1/H$  with  $H = 1, 2$  or  $3$ . There are uncertainties in the estimation of the toxicity values in the T. E. S. T. model evaluated according the different QSAR methodologies. Similarly, the proposed model must take into account the limits in the knowledge of the adverse outcome effects of some parameters. For some parameters of a fiber there is simply not enough experimental evidence to assess how and to what extent they produce adverse effects. The uncertainty U in the determination of the contribution of that specific parameter to the FPTI is accounted in the parameter  $w_2 = 1/U$  with  $U = 1$  (low to null uncertainty),  $2$  (some uncertainty), or  $3$  (high uncertainty).

Table 2 reports the values of H and U associated to each parameter of the model.

Having defined the weighing scheme of the parameters, the FPTI<sub>i</sub> of each fiber is calculated according to the following equation:

$$\text{FPTI}_i = \sum_{i=1}^n w_1 \cdot w_2 \cdot T_i$$

with  $T_i$  = class value of the  $i$  parameter of the model;  $w_1 = 1/H$  weight of the parameter according to its hierarchy H;  $w_2 = 1/U$  weight of the parameter according to the uncertainty U of its determination.

### 2.4. The classes of values for each parameter

Table 3 reports the classes of score assigned to each parameter FPTI<sub>i</sub>.

Some of the choices on the classes of score require an explanation. Concerning the length L, fibers shorter than  $5 \mu\text{m}$  were not considered as they are below the limit of regulated fibers according to the WHO (World Health Organization) (1997) criteria. The limit of  $10 \mu\text{m}$  was chosen because it is close to the value which defines a 'Stanton fiber' (Stanton et al., 1981) and is the mean upper limit of the diameter of the stomata which negotiates the fiber translocation outside the parietal pleura to the lymphatic system (Donaldson et al., 2010). The upper limit of  $20 \mu\text{m}$  was chosen because it is the mean maximum thickness of the pleural cavity so that fibers longer than  $20 \mu\text{m}$  can be trapped in that sac and prompt inflammatory activity.

Parameter (1,11) is  $\sum_i \frac{C_i}{L_i}$  = sum of the concentrations of heavy metals  $C_i$  in the fiber (in ppm) divided by the limit  $L_i$  for that metal according to the existing regulatory system. Heavy metals considered in the calculation are Sb, As, Hg, Cd, Co, Cr, Cu, Pb, Ni, Zn, V, Be; Be limit =  $0.5 \text{ ppm}$ , all the other limits are taken from Tóth et al. (2016).

Parameter (1,12) is the total dissolution time of the fiber calculated in years (y) following the standardized acellular *in vitro* dissolution model at pH = 4.5 (simulation of the intracellular environment in the phagolysosome) described in Gualtieri et al. (2018).

Parameter (1,13) is an estimate of the velocity of release of iron from the fiber into the cytoplasmic space during phagocytosis. Released iron can be active at the surface of the fiber and prompt the formation of hydroxyl radicals (Gualtieri et al., 2017). This parameter is calculated as the total content of elemental iron in the fiber (wt%) (which can be made available as active iron at the surface of the fiber) divided by the total dissolution time of the fiber, calculated in years (y) (see above). If the fiber dissolves fast, iron can be quickly made available at the surface of the fiber. In that case, the value of the parameter is  $> 1$  and the corresponding normalized score FPTI<sub>i</sub> is high (0.13), increasing the final score of the FPTI. Oppositely, if the fiber is biodegradable, iron release is slow. In that case, the value of the parameter is  $< 0.1$  and the corresponding normalized score FPTI<sub>i</sub> is low (0.03), decreasing the final score of the FPTI.

As it was experimentally observed (see for example Gualtieri et al., 2017), the dissolution of silicate mineral fibers produces an amorphous silica relict. The formation of a silica-rich fiber skeleton, characterized by silanol groups (Si–OH) and ionized silanol groups (Si–O<sup>−</sup>), may promote the production of hydroxyl radicals in synergy with surface iron species (Gualtieri et al., 2017). With this premise, the parameter (1,14) is an estimate of the rate of production of amorphous silica from the dissolving fiber inside the cytoplasmic space, calculated as the total content of elemental silicon in the fiber (wt%) divided by the total dissolution time (y) of the fiber (see above for the case of iron). Although this parameter has a great uncertainty (witnessed by the applied weighing factor), it is assumed that if the fiber dissolves fast, reactive amorphous silica surfaces are readily made available (the case of chrysotile). In that case, the value of the parameter is  $> 1$  and the corresponding normalized score FPTI<sub>i</sub> is high (0.07) and increases the final score of the FPTI. On the other hand, if the fiber is biodegradable, the formation of a reactive amorphous silica surface is slow. In this case, the assigned value of the parameter is  $< 0.5$  and the corresponding

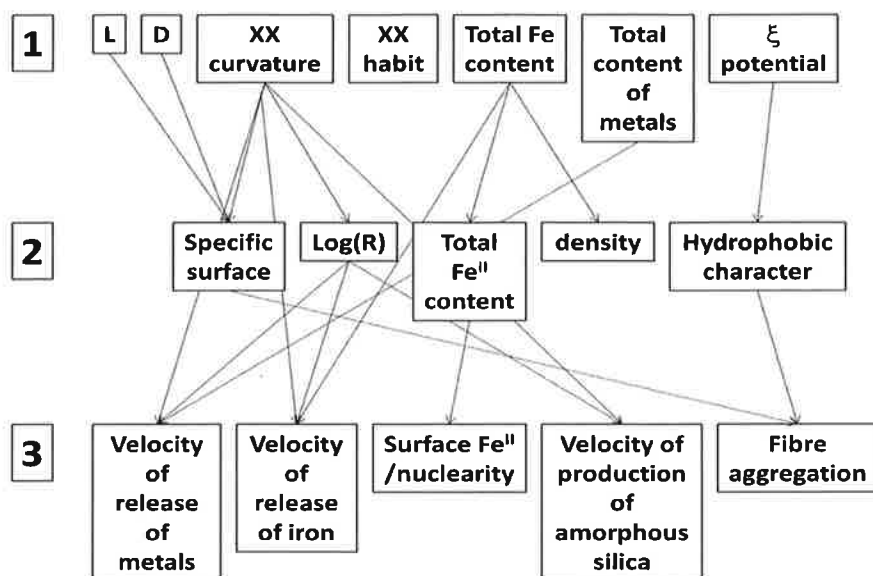


Fig. 1. Scheme of the hierarchical clustering in the FPTI model.

Table 2

The values of H (hierarchy) and U (uncertainty) associated to each parameter of the FPTI model.

Element	H	U
Morphometric		
(1,1)	1	1
(1,2)	1	1
(1,3)	1	2
(1,4)	1	1
(1,5)	2	1
(1,6)	2	1
(1,7)	2	1
Chemical		
(1,8)	1	2
(1,9)	2	1
(1,10)	3	2
(1,11)	1	1
Biodurability related		
(1,12)	2 <sup>a</sup>	1
(1,13)	3	1
(1,14)	3	2
(1,15)	3	1
Surface activity		
(1,16)	1	2
(1,17)	3	1
(1,18)	1	3

<sup>a</sup> already normalized with respect to the elements (1,1), (1,2), (1,8).

normalized score FPTIi is low (0.02).

Assuming that the dissolution of a fiber prompts the release of toxic/carcinogenic elements ("Trojan horse effect": Stern et al., 2012), parameter (1,15) is an estimate of the velocity of release of toxic elements from the dissolving fiber inside the cytoplasmic space, calculated as the total content (in ppm) of heavy metals (Sb, As, Hg, Cd, Co, Cr, Cu, Pb, Ni, Zn, V, Be; Mn, Be) divided by the total dissolution time (y) of the fiber (see above).

The error associated to each parameter is calculated from the propagation of the error associated to the experimental value.

### 3. Calculation of the FPTI

#### 3.1. Materials

The FPTI has been calculated for the following mineral fibers:

- amosite UICC asbestos standard (South African, NB #4173-111-4) with minor impurities of calcite, hematite and quartz;
- anthophyllite UICC standard asbestos (Finnish NB #4173-111-5). The sample is contaminated with biotite (1.4(2) wt%), clinocllore/vermiculite (1.7(3) wt%) and talc (7.7(4) wt%);
- chrysotile from Balangero (Torino, Italy) with impurities of antigorite, balangeroite, calcite, clinocllore, diopside, dolomite, magnetite, microcline, plagioclase, talc;
- chrysotile "B" asbestos UICC asbestos standard with impurities of brucite, calcite, clinocllore, dolomite, magnetite, microcline, pyroaurite and talc;
- chrysotile from Valmalenco (Sondrio, Italy) containing minor calcite, forsterite, magnetite, quartz, lizardite/antigorite, clinocllore;
- crocidolite UICC asbestos standard (South African, NB #4173-111-3) with minor impurities of hematite, magnetite, and quartz;
- fibrous erionite-Na from Jersey, Nevada (USA) with impurities of clinoptilolite;
- fibrous erionite-K from Karain, Cappadocia (Turkey) described in Dogan et al. (2008) and references therein;
- fibrous fluoro-edenite from Biancavilla, Sicilia (Italy) described in Gianfagna et al. (2003) and Andreozzi et al. (2009);
- fibrous sepiolite from Vallecas (Spain) described in Galan (1996);
- tremolite asbestos from Val d'Ala, Turin (Italy) with minor impurities of antigorite and clinocllore;
- wollastonite NYAD G well described in the IARC (2012) publication and Bellmann and Muhle (1994).

Physical-chemical data of erionite-K, fluoro-edenite, sepiolite and wollastonite were taken from the literature. More specific data like the  $\xi$  potential were extrapolated from other studies on these fibers. The other fibers were fully characterized in Pollastri et al. (2014, 2015).

#### 3.2. Examples of calculation

As example, the FPTI has been calculated for Balangero's chrysotile

**Table 3**  
The weighing score associated to each parameter of the FPTI model.

Element	Classes	Normalized score FPTI <sub>i</sub>
<b>Morphometric</b>		
(1,1)	> 5μm and < 10μm	0.1
	> 10μm and < 20μm	0.2
	> 20μm	0.4
(1,2)	> 1μm and < 3μm	0.1
	> 0.25μm and < 1μm	0.2
	> 0.25μm	0.4
(1,3)	Flat surface (perfect crystal)	0.05
	Altered surface	0.1
	Cylindrical surface	0.2
(1,4)	Curled	0.1
	Mixed Curled/acicular	0.2
	Acicular	0.4
(1,5)	< 2.75 g/cm <sup>3</sup>	0.05
	> 2.75 and < 3.5 g/cm <sup>3</sup>	0.1
	> 3.5 g/cm <sup>3</sup>	0.2
(1,6)	Hydrophobic	0.05
	Amphiphilic	0.1
	Hydrophilic	0.2
(1,7)	> 25 m <sup>2</sup> /g	0.05
	< 25 and > 5 m <sup>2</sup> /g	0.1
	< 5 m <sup>2</sup> /g	0.2
<b>Chemical</b>		
(1,8)	Fe <sub>2</sub> O <sub>3</sub> + FeOwt% < 1	0.05
	1 < Fe <sub>2</sub> O <sub>3</sub> + FeOwt% < 10	0.1
	Fe <sub>2</sub> O <sub>3</sub> + FeOwt% > 10	0.2
(1,9)	0 < FeOwt% < 0.25	0.05
	0.25 < FeOwt% < 1	0.1
	FeOwt% > 1	0.2
(1,10)	Fe <sup>2+</sup> nuclearity > 2	0.02
	Fe <sup>2+</sup> nuclearity = 2	0.03
	Fe <sup>2+</sup> nuclearity = 1	0.07
(1,11) <sup>a</sup>	$\sum_i \frac{C_i}{L_i} < 1$	0.1
	$1 < \sum_i \frac{C_i}{L_i} < 5$	0.2
	$\sum_i \frac{C_i}{L_i} > 5$	0.4
<b>Biodurability related</b>		
(1,12) <sup>a</sup>	< 1 y	0.05
	> 1 and < 40 y	0.1
	> 40 y	0.2
(1,13) <sup>a</sup>	< 0.1	0.03
	> 0.1 and < 1	0.07
	> 1	0.13
(1,14) <sup>a</sup>	< 0.5	0.02
	> 0.5 and < 1	0.03
	> 1	0.07
(1,15) <sup>a</sup>	< 1	0.03
	> 1 and < 10	0.07
	> 10	0.13
<b>Surface activity</b>		
(1,16)	Negative at pH = 4.5 (intracellular)	0.1
	Negative at both pH = 4.5 and 7 (intracellular and extracellular)	0.2
(1,17)	$\zeta >  20 $	0.03
	$ 10  < \zeta <  20 $	0.07
	$ 0  < \zeta <  10 $	0.13
(1,18)	Cation exchange (zeolite)	0.07
	No cation exchange (no zeolite)	0

<sup>a</sup> The definition of the parameter is explained in the text.

and for tremolite from Val d'Ala. The same model has been applied to all the other fibers selected in this study. The calculated figures are reported in Table 4.

#### 4. Results and discussion

Because a number of the parameters which characterize the fibers are measured *ex situ*, the model that has been developed is based in part

**Table 4**

The parameters used and the calculated FPTI for the chrysotile sample from Balangero and the tremolite asbestos sample from Val d'Ala.

Morphometric element	FPTI <sub>i</sub>	
Sample	Chrysotile, Balangero (Italy)	Asbestos tremolite, Val D'Ala (Italy)
(1,1)	0.4	0.4
(1,2)	0.1	0.1
(1,3)	0.2	0.1
(1,4)	0.1	0.4
(1,5)	0.05	0.1
(1,6)	0.2	0.2
(1,7)	0.05	0.2
<b>Chemical</b>		
(1,8)	0.05	0.1
(1,9)	0.2	0.2
(1,10)	0.03	0.03
(1,11)	0.4	0.4
<b>Biodurability related</b>		
(1,12)	0.05	0.2
(1,13)	0.07	0.07
(1,14)	0.067	0.03
(1,15)	0.133	0.13
<b>Surface activity</b>		
(1,16)	0.1	0.2
(1,17)	0.033	0.07
(1,18)	0	0
FPTI (error)	2.23(0.21)	2.88(0.43)

on parameters measured in artificial conditions that are quite different from those that exist in the lung. Further experimental data are in progress to verify the toxic/pathogenic effects of the parameters predicted by the model and the creation of a representative database of mineral fibers so to accomplish a more judicious selection and rationale of the numerous hypothetical influential variables of the model. Notwithstanding, the present model conveys FPTI values fibers (see Table 5 reporting the FPTI values with the estimated error in parenthesis) that allow a quantitative comparison of the toxicity/pathogenicity potential of the investigated mineral fibers. The first column reports the FPTI value for the raw fibers whereas the second column reports the value normalized with respect to the morphometric parameters, i.e. assuming the same morphometric parameters ( $L > 20$  mm,  $D < 0.25$  mm) and consequently the corresponding FPTI<sub>i</sub> values (0.4 and 0.4) for all the fibers. Fig. 2 plots the results of Table 5 so that a direct comparison is possible and classes of FPTI values can be drawn.

**Table 5**

FPTI of the mineral fibers selected in this study.

Sample	FPTI raw fiber	FPTI normalized morphometry <sup>a</sup>
Amosite UICC	3.17(0.11)	3.17(0.11)
Tremolite Val Ala (Italy)	2.88(0.43)	3.18(0.43)
Anthophyllite UICC	2.78(0.12)	2.93(0.12)
Crocidolite UICC	2.67(0.11)	2.87(0.11)
Fluoro-edenite Biancavilla (Italy)	2.59(0.31)	2.79(0.31)
Fibrous erionite Jersey (USA)	2.35(0.19)	2.75(0.19)
Fibrous erionite Karain (Turkey)	2.33(0.23)	2.73(0.23)
Chrysotile Balangero (Italy)	2.23(0.21)	2.53(0.21)
Chrysotile Val Malenco (Italy)	2.14(0.26)	2.54(0.26)
Chrysotile UICC	2.18(0.11)	2.38(0.11)
Wollastonite NYAD G (USA)	1.92(0.30)	2.42(0.30)
Fibrous sepiolite Vallecas (Spain)	1.68(0.11)	1.98(0.11)

<sup>a</sup> FPTI was calculated assuming the same morphometric parameters for all the fibers with  $L > 20$  mm,  $D < 0.25$  mm.

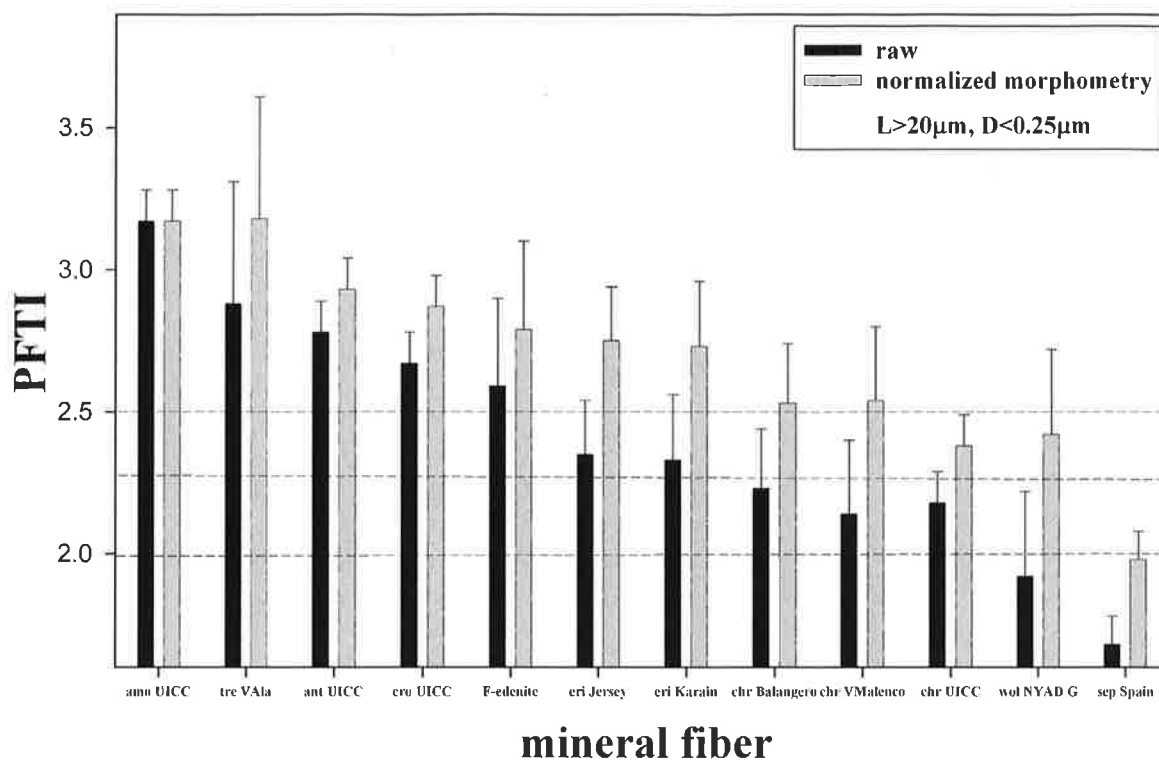


Fig. 2. The calculated FPTI for the investigated mineral fibers.

The classification of the investigated mineral fibers is based upon their harmful adverse effects (Costa and Fadeel, 2016) in the body and collectively takes into account all the factors responsible for cytotoxicity, primary and secondary genotoxicity, pathogenicity (carcinogenicity). Here, the latter specifically refers to the ability of a fiber to act as lung cancer and MM inducing agent following chronic inhalation.

Fig. 2 evidences that there are differences among the different fiber species. Indicatively, all the amphibole asbestos species display FPTI values > 2.50 (the upper dashed black line), fibrous erionite samples display FPTI values in the range 2.30–2.50 (the middle dashed black line) whereas chrysotile asbestos samples have values in the range 2.00–2.30. FPTI values < 2.00 regard mineral fibers that have been considered as negative standards (fibers that according to the literature data do not display harmful effects). In fact, IARC (2012) monographs report that there is inadequate evidence in humans for the carcinogenicity of fibrous wollastonite and sepiolite (Group 3). This model quantitatively supports the concept of a difference of toxicity/pathogenicity potential of amphibole asbestos with respect to chrysotile asbestos based on their physical/chemical/structural properties. The calculated mean FPTI of the four investigated amphibole asbestos (amosite, anthophyllite, crocidolite and tremolite) is 2.88(0.19) which is significantly higher than the value 2.18(0.19) corresponding to the mean FPTI of the three chrysotile asbestos samples. For sure, the difference in the measured biodegradability of these two fibers has a great influence as already remarked in the literature. As a matter of fact, the lack of biopersistence of chrysotile causing it to disintegrate and become shorter in the lungs is the main structural feature that leads to chrysotile being less pathogenic than the amphiboles (Hodgson and Darnton, 2000). Notwithstanding, both indices for amphibole and chrysotile asbestos are significantly higher than the threshold limit (indicatively set at 2.00) set for 'safe' mineral fibers wollastonite and sepiolite. Fibrous erionite displays a mean FPTI of 2.34(0.22) in between the amphibole and chrysotile asbestos values. The prediction apparently contradicts the proviso that erionite is considered one of the most toxic minerals known (Dogan et al., 2008) and that is 500–800

times more tumorigenic than chrysotile (Coffin et al., 1992). Besides the fact that, oppositely to toxicity which relies upon a dose, addressing a quantitative rank to the tumorigenic (carcinogenic) potential is an undefined concept, Coffin et al. (1992) themselves recognize that a factor they termed 'intrinsic potency', probably related to surface activity, overrides both fiber number and geometric configuration. This potency difference may be related to differing tendencies of the respective surfaces to coordinate endogenous iron and release hydroxyl radicals via the Fenton reactions (Coffin et al., 1992). The prediction of these authors is housed in the FPTI model where the role of such chemical/structural parameters is pivotal but the quantitative result points to a possible different scenario: the supposed amplification of the toxicity potential of fibrous erionite with respect to other harmful mineral fibers resides in exogenous factors other than fiber characteristics, namely genetic susceptibility to MM of the population that came in contact with that fiber (Dogan et al., 2006; Carbone et al., 2007).

The normalization of the morphometric parameters ( $L > 20 \mu\text{m}$ ,  $D < 0.25 \mu\text{m}$ ) for the group of investigated fibers (gray bars in Fig. 2) does not appreciably change the rank observed for the raw fibers except for the wollastonite NYAD G fiber whose index shifts from 1.92 (in the region of safe fibers) to 2.42 (in the region of harmful fibers). This finding is highly informative as: (i) it stresses out the major importance of the size-related parameters in the FPTI model; as a matter of fact, together with biodegradability,  $L$  and  $D$  are the bearing walls of the 'fiber paradigm'; (ii) even safe natural fiber species like wollastonite may virtually display toxicity/pathogenicity potential if their morphometric parameters exceed the threshold values. Providentially, real wollastonite fibers with such size characteristics are not found in nature due to their peculiar geological conditions of formation (minerogenesis). In fact, in natural wollastonite, even the smallest individual particles commonly exhibit a maximum aspect ratio of 7:1 or 8:1 and have an average diameter of  $3.5 \mu\text{m}$  (Bauer et al., 1994). On the other hand, the issue is still open for synthetic wollastonite fibers which may display morphometric parameters so that their potential toxicity/pathogenicity index increases. The same proviso apply to other fiber species with their natural and synthetic counterparts.

## 5. Conclusions

A first attempt to devise a quantitative predictive model of toxicity/pathogenicity of minerals fibers based on their physical/chemical and morphological parameters is presented. The author recognizes that the model presented is based in part on parameters measured in artificial conditions that are quite different from those that exist in the lung and is aware that there is current research to provide new measurements which better simulate the lung's environment.

The model permits to calculate a fiber potential toxicity/pathogenicity index (FPTI) which can be a useful tool to interpret the results of *in vitro* and *in vivo* testing. The paper evidences both advantages and weak spots of the model to be further investigated. The latter include the nature of the surface chemical activity (e.g. iron activity) which can be affected by the protein corona formed around the fiber.

In order to optimize and validate the proposed model, work is in progress to:

- collect new experimental data aimed at the verification of the toxic/pathogenic effects of the parameters predicted by the model and creation of a representative database of mineral fibers;
- improve the model to accomplish a more judicious selection and rationale of the numerous hypothetical influential variables and optimization of the algorithms for the estimation of the weights of each macro-/micro-parameter terms;
- develop a model-based user-friendly code to assess the toxicity/pathogenicity of a fiber;
- validate the model at international level and evaluate the social, economic and legal consequences of the obtained results.

The application of the model to fibers of environmental, social and economic importance allowed to establish different classes of potential toxicity/pathogenicity with the amphibole fibers that appear by far as the most harmful fiber species. The findings confirm the famous deduction of Paracelsus (1493–1541) “the dose makes the poison (*sola dosit facit venenum*)” which is the basic principle of toxicology: “All things are poison and nothing is without poison; only the dose makes a thing not a poison”. In the specific case of mineral fibers such principle can be possibly reworded as: “All fibers are poison; only the *structural (s.L.)* characters and the dose makes a fiber (not) a poison”.

## Conflict of interest statement

The author declares that there are no conflicts of interest.

## Acknowledgements

This work has been supported by the National Grant PRIN2010 and would have not been possible without the contribution of the scientists involved in the long term project on mineral fibers, namely Giovanni B. Andreozzi, Fiorella Belpoggi, Andrea Bloise, Nicola Bursi Gandolfi, Eva Magdalena Lassinantti Gualtieri, Simone Pollastri, Armanda Pugnali, Eva Tibaldi, and Ruggero Vigliaturo. This manuscript greatly benefited from the fruitful discussions and critical revision of Dr. David Bernstein and Dr. Annie Jarabek. The author also wishes to thank the two competent referees for their work that certainly improved the quality of the manuscript.

## References

Andreozzi, G.B., Ballirano, P., Gianfagna, A., Mazziotti-Tagliani, S., Pacella, A., 2009. Structural and spectroscopic characterization of a suite of fibrous amphiboles with high environmental and health relevance from Biancavilla (Sicily, Italy). *Am. Mineral.* 94 (10), 1333–1340.

Ballirano, P., Cametti, G., 2015. Minerals in the human body. Crystal chemical and structural modifications of erionite fibers leached with simulated lung fluids. *Am. Mineral.* 100 (4), 1003–1012.

Bauer, R.R., Copeland, H.R., Santini, K., 1994. Wollastonite, Ind. Min. Rocks 1119–1128.

Baumann, F., Ambrosi, J.P., Carbone, M., 2013. Asbestos is not just asbestos: an unrecognised health hazard. *Lancet Oncol.* 14 (7), 576–578.

Bellmann, B., Muhle, H., 1994. Investigation of the biodegradability of wollastonite and xonotlite. *Environ. Health Perspect.* 102 (5), 191–195.

Bernstein, D., Pavlisko, E.N., 2017. Differential pathological response and pleural transport of mineral fibres. Chapter 12. In: Gualtieri, A.F. (Ed.), *Mineral fibres: crystal chemistry, chemical-physical properties, biological interaction and toxicity*. EMU Notes in Mineralogy 18, pp. 417–434.

Bernstein, D.M., Donaldson, K., Decker, U., Gaering, S., Kunzendorf, P., Chevalier, J., Holm, S.E., 2008. A biopersistence study following exposure to chrysotile asbestos alone or in combination with fine particles. *Inhal. Toxicol.* 20, 1009–1028.

Bernstein, D., Dunnigan, J., Hesterberg, T., Brown, R., Velasco, J.A.L., Barrera, R., Hoskins, J., Gibbs, A., 2013. Health risk of chrysotile revisited. *Crit. Rev. Toxicol.* 43 (2), 154–183.

Berry, G., Newhouse, M.L., 1983. Mortality of workers manufacturing friction materials using asbestos. *Occup. Environ. Med.* 40 (1), 1–7.

Bignon, J., Jaurand, M.C., 1983. Biological *in vitro* and *in vivo* responses of chrysotile versus amphiboles. *Environ. Health Perspect.* 51, 73–80.

Bloise, A., Barca, D., Gualtieri, A.F., Pollastri, S., Belluso, E., 2016. Trace elements in hazardous mineral fibres. *Environ. Pollut.* 216, 314–323.

Brunauer, S., Emmett, P.H., Teller, E., 1938. Adsorption of gases in multimolecular layers. *J. Am. Chem. Soc.* 60 (2), 309–319.

Bursi Gandolfi, N., Gualtieri, A.F., Pollastri, S., Tibaldi, E., Belpoggi, F., 2016. Assessment of asbestos body formation by high resolution FEG–SEM after exposure of Sprague–Dawley rats to chrysotile, crocidolite, or erionite. *J. Hazard. Mater.* 306, 95–104.

Carbone, M., Emri, S., Dogan, A.U., Steele, L., Tuncer, M., Pass, H.L., Baris, Y.L., 2007. A mesothelioma epidemic in Cappadocia: scientific developments and unexpected social outcomes. *Nat. Rev. Cancer* 7, 147–154.

Churg, A., 1993. Asbestos lung burden and disease patterns in man. In: Guthrie, G.D., Mossman, B.T. (Eds.), *Health Effects of Mineral Dust*. Rev. in Min. and Geochem. 28, Mineralogical Society of America, Chantilly, Virginia, USA, pp. 409–426.

Coffin, D.L., Cook, P.M., Creason, J.P., 1992. Relative mesothelioma induction in rats by mineral fibers: comparison with residual pulmonary mineral fiber number and epidemiology. *Inhal. Toxicol.* 4 (3), 273–300.

Costa, P.M., Fadeel, B., 2016. Emerging systems biology approaches in nanotoxicology: Towards a mechanism-based understanding of nanomaterial hazard and risk. *Tox. App. Pharm.* 299, 101–111.

DeLoid, G., Cohen, J.M., Darrah, T., Derk, R., Wang, L., Pyrgiotakis, G., Wohlleben, W., Demokritou, P., 2014. Estimating the effective density of engineered nanomaterials for *in vitro* dosimetry. *Nat. Commun.* 5, 3514.

Deng, Z.J., Liang, M.L., Tóth, I., Monteiro, M.J., Michin, R.F., 2012. Molecular interaction of poly(acrylic acid) gold nanoparticles with human fibrinogen. *ACS Nano* 6, 8962–8969.

Dixon, J.R., Lowe, D.B., Richards, D.E., Cralley, L.J., Stokinger, H.E., 1970. The role of trace metals in chemical carcinogenesis: asbestos cancers. *Cancer Res.* 30, 1068–1074.

Dogan, A.U., Baris, Y.L., Dogan, M., Emri, S., Steele, L., Elmishad, A.G., Carbone, M., 2006. Genetic predisposition to fiber carcinogenesis causes a mesothelioma epidemic in Turkey. *Cancer Res.* 66 (10), 5063–5068.

Dogan, A.U., Dogan, M., Hoskins, J.A., 2008. Erionite series minerals: mineralogical and carcinogenic properties. *Environ. Geochem. Health* 30, 367–381.

Donaldson, K., Murphy, F.A., Duffin, R., Poland, C.A., 2010. Asbestos, carbon nanotubes and the pleural mesothelium: a review of the hypothesis regarding the role of long fibre retention in the parietal pleura, inflammation and mesothelioma. *Part. Fibre Tox.* 7, 5.

Evans, J.C., Evans, R.J., Holmes, A., Hounam, R.F., Jones, D.M., Morgan, A., Walsh, M., 1973. Studies on the deposition of inhaled fibrous material in the respiratory tract of the rat and its subsequent clearance using radioactive tracer techniques: 1. UICC crocidolite asbestos. *Environ. Res.* 6, 180–201.

Fischer, C., Kurganskaya, I., Schäfer, T., Lüttge, A., 2014. Variability of crystal surface reactivity: what do we know? *Appl. Geochem.* 43, 132–157.

Gabor, S., Anca, Z., 1975. Effect of asbestos on lipid peroxidation in the red cells. *Brit. J. Ind. Med.* 32, 39–41.

Galan, E., 1996. Properties and applications of palygorskite-sepiolite clays. *Clay Miner.* 31 (4), 443–453.

Gianfagna, A., Ballirano, P., Bellatreccia, F., Bruni, B., Paoletti, L., Oberti, R., 2003. Characterization of amphibole fibres linked to mesothelioma in the area of Biancavilla, Eastern Sicily, Italy. *Min. Mag.* 67 (6), 1221–1229.

Gualtieri, A.F., Artioli, G., Passaglia, E., Bigi, S., Viani, A., Hanson, J.C., 1998. Crystal structure-crystal chemistry relationships in the zeolites erionite and offretite. *Am. Mineral.* 83, 590–606.

Gualtieri, A.F., Mossman, B.T., Roggli, V.L., 2017. Towards a general model for predicting the toxicity and pathogenicity of mineral fibres. Chapter 15. In: Gualtieri, A.F. (Ed.), *Mineral Fibres: Crystal Chemistry, Chemical-Physical Properties, Biological Interaction and Toxicity*. EMU Notes in Mineralogy 18, pp. 501–532.

Gualtieri, A.F., Pollastri, S., Bursi Gandolfi, N., Lassinantti Gualtieri, M., 2018. Dissolution of mineral fibres. A comparative acellular *in vitro* study. *Sci. Rep.* (7071).

Halliwel, B., 1990. How to characterize a biological antioxidant. *Free Radic. Res. Commun.* 9 (1), 1–32.

Hardy, J.A., Aust, E., 1995. Iron in asbestos chemistry and carcinogenicity. *Chem. Rev.* 95, 97–118.

Harris, R.L., Timbrell, V., 1977. Relation of alveolar deposition to the diameter and length of glass fibres. In: *Proceedings of the Inhaled Particles IV*. Proc. Int. Symp. British Occ. Hyg. Soc., Edinburgh, 1977, Pergamon Press Oxford, pp. 411.

- Harrison, P.T., Levy, L.S., Patrick, G., Pigott, G.H., Smith, L.L., 1999. Comparative hazards of chrysotile asbestos and its substitutes: a European perspective. *Environ. Health Perspect.* 107 (8), 607–611.
- Hawthorne, F.C., Oberti, R., Harlow, G.E., Maresch, W.V., Martin, R.F., Schumacher, J.C., Welch, M.D., 2012. Nomenclature of the amphibole supergroup. *Am. Mineral.* 97, 2031–2048.
- Hodgson, J.T., Darnton, A., 2000. The quantitative risks of mesothelioma and lung cancer in relation to asbestos exposure. *Ann. Occup. Hyg.* 44, 565–601.
- IARC, 2012. Arsenic, metals, fibres and dusts: a review of human carcinogens. In: *Proceedings of the IARC Working Group on the Evaluation of Carcinogenic Risks to Humans*, Lyon, France. International Agency for Research on Cancer, pp. 501.
- Ilgren, E., 2008. Coalinga chrysotile: dissolution, concentration, regulation and general relevance. *Indoor Built Env.* 17, 42–57.
- Ilgren, E., Chatfield, E., 1998. Coalinga fibre, a short, amphibole-free chrysotile. Part 2: evidence for lack of tumourigenic activity. *Indoor Built Env.* 7, 18–31.
- Kamp, D.W., 2009. Asbestos-induced lung diseases: an update. *Transl. Res.* 153, 143–152.
- Kostarelos, K., 2008. The long and short of carbon nanotube toxicity. *Nat. Biotechnol.* 26, 774–776.
- Lynch, I., Dawson, K.A., 2008. Protein-nanoparticle interactions. *Nano Today* 3, 40–47.
- Marques, M.R.C., Loebenberg, R., Almukainzi, M., 2011. Simulated biological fluids with possible application in dissolution testing. *Dissol. Tech.* 18 (3), 15–28.
- Munn, M.D., Gilliom, R.J., Moran, P.W., Nowell, L.H., 2001. Pesticide Toxicity Index for Freshwater Aquatic Organisms. US Department of the Interior, US Geological Survey.
- Nemery, B., 1990. Metal toxicity and the respiratory tract. *Eur. Respir. J.* 3, 202–219.
- Nowell, L.H., Norman, J.E., Moran, P.W., Martin, J.D., Stone, W.W., 2014. Pesticide toxicity index—a tool for assessing potential toxicity of pesticide mixtures to freshwater aquatic organisms. *Sci. Total Environ.* 476, 144–157.
- Papa, E., Dearden, J.C., Gramatica, P., 2007. Linear QSAR regression models for the prediction of bioconcentration factors by physicochemical properties and structural theoretical molecular descriptors. *Chemosphere* 67 (2), 351–358.
- Pollastri, S., Gualtieri, A.F., Gualtieri, M.L., Hanuskova, M., Cavallo, A., Gaudino, G., 2014. The zeta potential of mineral fibres. *J. Hazard. Mater.* 276, 469–479.
- Pollastri, S., D'Acapito, F., Trapananti, A., Colantoni, L., Andreozzi, G.B., Gualtieri, A.F., 2015. The chemical environment of iron in mineral fibres. A combined X-ray absorption and Mossbauer spectroscopic study. *J. Hazard. Mater.* 298, 282–293.
- Pollastri, S., Gualtieri, A.F., Ignatyev, K., Straffella, E., Pugnali, A., Croce, A., 2016. Stability of mineral fibres in contact with human cell cultures. An in situ  $\mu$ XANES,  $\mu$ XRD and XRF iron mapping study. *Chemosphere* 164, 547–557.
- Roggli, V.L., Sharma, A., 2014. Analysis of tissue mineral fiber content. In: *Pathology of Asbestos-Associated Diseases*. Springer Berlin Heidelberg, pp. 253–292.
- Roy, K., Das, R.N., 2013. QSTR with extended topochemical atom (ETA) indices. 16. Development of predictive classification and regression models for toxicity of ionic liquids towards *Daphnia magna*. *J. Hazard. Mater.* 254, 166–178.
- Rufe, E., Hochella Jr., M.F., 1999. Quantitative assessment of reactive surface area of phlogopite during acid dissolution. *Science* 285, 874–876.
- Sayan, M., Mossman, B.T., 2017. Erionite and asbestos in the pathogenesis of human malignant mesotheliomas. In: *The Molecular Basis of Human Cancer*, Springer, New York, pp. 287–295.
- Stanton, M.F., Layard, M., Tegeris, A., Miller, E., May, M., Morgan, E., Smith, A., 1981. Relation of particle dimension to carcinogenicity in amphibole asbestos and other fibrous minerals. *J. Natl. Cancer Inst.* 67, 965–975.
- Stern, S.T., Adiseshaiah, P.P., Crist, R.M., 2012. Autophagy and lysosomal dysfunction as emerging mechanisms of nanomaterial toxicity. *Part. Fibre Tox.* 9 (1), 20.
- Tóth, G., Hermann, T., Da Silva, M.R., Montanarella, L., 2016. Heavy metals in agricultural soils of the European Union with implications for food safety. *Environ. Int.* 88, 299–309.
- Turci, F., Tomatis, M., Lesci, L.G., Roveri, N., Fubini, B., 2011. The iron-related molecular toxicity mechanism of synthetic asbestos nanofibres: a model study for high aspect ratio nanoparticles. *Chemistry* 17, 350–358.
- U.S. Environmental Protection Agency (EPA), 2012. USEPA T. E. S. T. Tool, User's Guide for T.E.S.T.
- Utembe, W., Potgieter, K., Stefaniak, A.B., Gulmian, M., 2015. Dissolution and biodegradability: important parameters needed for risk assessment of nanomaterials. *Part. Fibre Tox.* 12 (1), 11.
- van Oss, C.J., Naim, J.O., Costanzo, P.M., Giese, R.F., Wu, W., Sorling, A.F., 1999. Impact of different asbestos species and other mineral particles on pulmonary pathogenesis. *Clay Clay Miner.* 47, 697–707.
- Wei, B., Yang, L., Zhu, O., Yu, J., Jia, X., 2014. Multivariate analysis of trace elements distribution in hair of pleural plaques patients and health group in a rural area from China. *Hair* 4, 2167–3118.
- WHO (World Health Organization), 1997. Determination of Airborne Fibre Number Concentrations. <http://apps.who.int/iris/bitstream/10665/41904/1/9241544961.pdf>, Accessed date: 23 May 2017.
- Wypych, F., Adad, L.B., Mattoso, N., Marangon, A.A., Schreiner, W.H., 2005. Synthesis and characterization of disordered layered silica obtained by selective leaching of octahedral sheets from chrysotile and phlogopite structures. *J. Colloid Interface Sci.* 283, 107–112.
- Yeh, H.C., Phalen, R.F., Raabe, O.G., 1976. Factors influencing the deposition of inhaled particles. *Environ. Health Perspect.* 15, 147–156.
- Zecchina, A., Rivalan, M., Berlier, G., Lamberti, C., Ricchiardi, G., 2007. Structure and nuclearity of active sites in Fe-zeolites: comparison with iron sites in enzymes and homogeneous catalysts. *Phys. Chem. Chem. Phys.* 9, 3483–3499.
- Zhang, D.K., Li, R.S., Han, X., Li, C.Y., Zhao, Z.H., Zhang, H.Z., Yang, M., Wang, J.B., Xiao, X.H., 2016. Toxic Constituents Index: A toxicity-calibrated quantitative evaluation approach for the precise toxicity prediction of the hypertoxic phytochemistry—Aconite. *Front. in Pharm.* 7, 164–176.